



Methylglyoxal suppresses microglia inflammatory response through NRF2-IκBζ pathway

Shu-Li Wei^a, Ying Yang^b, Wei-Yue Si^a, Yang Zhou^c, Tao Li^c, Tong Du^{c,d}, Peng Zhang^{c,d}, Xiao-Li Li^{c,d}, Ruo-Nan Duan^e, Rui-Sheng Duan^{a,c,d,**}, Chun-Lin Yang^{c,d,*}

^a Department of Neurology, Shandong Provincial Qianfoshan Hospital, Shandong University, Jinan 250011, PR China

^b Department of Pharmacy, The Affiliated Hospital of Shandong University of Traditional Chinese Medicine, Jinan, 250014, China

^c Department of Neurology, The First Affiliated Hospital of Shandong First Medical University, Jinan 250014, PR China

^d Shandong Institute of Neuroimmunology, Jinan 250014, PR China

^e Department of Neurology, Qilu Hospital, Cheeloo College of Medicine, Shandong University, Jinan, Shandong, 250012, China

ARTICLE INFO

Keywords:

Microglia
Methylglyoxal
Experimental autoimmune encephalomyelitis (EAE)
Nuclear factor erythroid 2-related factor 2 (NRF2)

ABSTRACT

Methylglyoxal (MGO) is a highly reactive metabolite generated by glycolysis. Although abnormal accumulation of MGO has been reported in several autoimmune diseases such as multiple sclerosis and rheumatoid arthritis, the role of MGO in autoimmune diseases has not yet been fully investigated. In this study, we found that the intracellular MGO levels increased in activated immune cells, such as microglia and lymphocytes. Treatment with MGO inhibited inflammatory cell accumulation in the spinal cord and ameliorated the clinical symptoms in EAE mice. Further analysis indicated that MGO suppressed M1-polarization of microglia cells and diminished their inflammatory cytokine production. MGO also inhibited the ability of microglial cells to recruit and activate lymphocytes by decreasing chemokine secretion and expression of co-stimulatory molecules. Furthermore, MGO negatively regulated glycolysis by suppressing glucose transporter 1 expression. Mechanically, we found that MGO could activate nuclear factor erythroid 2-related factor 2 (NRF2) pathway and NRF2 could bind to the promoter of IκBζ gene and suppressed its transcription and subsequently pro-inflammatory cytokine production. In conclusion, our results showed that MGO acts as an immunosuppressive metabolite by activating the NRF2-IκBζ.

1. Introduction

Multiple sclerosis (MS) is a major neuroinflammatory, demyelinating, and neurodegenerative disease of the central nervous system (CNS) characterized by inflammatory cell infiltration, demyelination, axonal loss, and gliosis [1]. Both CNS-resident immune cells, such as microglia, and infiltrated immune cells (including macrophages and T and B lymphocytes) play crucial roles in the pathogenesis of MS [2,3]. Therefore, understanding the underlying mechanism of immune processes during MS progression is the cornerstone for the identification of novel disease-modifying drugs.

After activation, immune cells engage in metabolic remodeling to support the energy and biosynthetic demands for proliferation and effector functions [4]. Notably, boosted glucose uptake and flux through glycolysis are common metabolic features of different immune cells [4].

In particular, targeted glycolysis has been shown to profoundly affect immune responses, including infections, inflammation, and autoimmune diseases [4–6]. However, the underlying mechanisms of metabolism and immune regulation remain unclear. Previous studies have illustrated the immune-regulatory effects of endogenous metabolites generated from glycolysis, the tricarboxylic acid (TCA) cycle, and amino acid metabolism, which include lactate [7], itaconate, succinate [8]. These metabolites profoundly impact immune reactions by binding to high-affinity receptors, post-translational modifications (PTMs) of target proteins, or unexplained mechanisms. For example, succinate, produced by macrophages after activation with lipopolysaccharide (LPS), stabilizes the transcription factor hypoxia-inducible factor 1α (HIF-1α) and subsequently enhances IL-1β production [8]. On the other hand, lactate, generated through aerobic glycolysis in tumors, polarizes macrophages to an anti-inflammatory phenotype that expresses genes encoding

* Corresponding author. Department of Neurology, The First Affiliated Hospital of Shandong First Medical University, Jinan 250014, PR China.

** Corresponding author. Department of Neurology, Shandong Provincial Qianfoshan Hospital, Shandong University, Jinan 250011, PR China.

E-mail addresses: ruisheng_duan@163.com (R.-S. Duan), muyilin1991@163.com (C.-L. Yang).

<https://doi.org/10.1016/j.redox.2023.102843>

Received 7 July 2023; Received in revised form 5 August 2023; Accepted 6 August 2023

Available online 8 August 2023

2213-2317/© 2023 The Authors. Published by Elsevier B.V. This is an open access article under the CC BY-NC-ND license (<http://creativecommons.org/licenses/by-nc-nd/4.0/>).

products critical for tumor growth [7].

Methylglyoxal (MGO) is a highly reactive carbonyl species mainly generated from the glycolytic intermediates, glyceraldehyde 3-phosphate (GA3P) and dihydroxyacetone phosphate (DHAP), in a nonenzymatic manner [9]. It has been estimated that 0.1–0.4% of the glycolytic flux results in MGO production [10]. Thus, it is easy to interpret that immune cells with higher glycolysis rate will produce larger amount of MGO. Indeed, MGO is upregulated in LPS-activated macrophages, which has high rate of glycolysis [11]. Additionally, excessive accumulation of MGO has been reported in various conditions, including diabetes, cancer, neurodegenerative and inflammatory diseases such as MS, and rheumatoid arthritis (RA) [12–16]. Due to its highly reactive electrophilic nature, MGO can spontaneously form covalent bonds with various biomolecules, such as nucleic acids and proteins, and affect several physiological and pathological processes [9]. Over the past decades, numerous studies have focused on elucidating the role of MGO in aging-related diseases, such as diabetes, cancer, and neurodegenerative diseases [12–14]. However, the roles and mechanisms of MGO in inflammatory diseases are still not fully understood.

Therefore, in this study, we observed that activated immune cells showed elevated levels of MGO accumulation. Specifically, MGO treatment inhibits microglial cell activation and restrains CNS autoimmunity in a mouse model of experimental autoimmune encephalomyelitis (EAE). Furthermore, MGO mechanistically activated the nuclear factor erythroid 2-related factor 2 (NRF2) antioxidant pathway and subsequently reduced M1 polarization and pro-inflammatory cytokine production in microglial cells.

2. Materials and methods

2.1. Animals

C57BL/6 J mice aged 7–8 weeks were obtained from Shandong Baipeng Biotechnology Co., Ltd. They were housed in a specific pathogen-free (SPF) facility with a 12 h light/dark cycle with free access to food and water. All animal experimental procedures were reviewed and approved by the Institutional Animal Care and Use Committee of the First Affiliated Hospital of Shandong First Medical University.

2.2. EAE induction and treatment

EAE was induced according to previously established methods [17, 18]. Briefly, mice were subcutaneously immunized with 200 mg MOG 35–55 peptide emulsified in complete Freund's adjuvant containing 0.4 mg *Mycobacterium tuberculosis* H37 Ra (BD Difco) and intraperitoneally injected with 200 ng pertussis toxin (List Biological Laboratories) on days 0 and 2 post-immunization. The mice were randomly divided into MGO and control groups which were treated with 500 mg/kg MGO (dissolved in water) or equal volume of vehicle (water) twice a day at 10 days post immunization. Clinical evaluation was performed daily as follows: 0, no clinical signs; 1, limp tail; 2, limp tail, impaired righting reflex, and paresis of one limb; 3, hind limb paralysis; 4, hind limb and forelimb paralysis; and 5, moribund.

2.3. Cell culture

BV2 mouse microglia cells were obtained from Procell Life Science & Technology Co., Ltd. (Wuhan, China) and cultured in minimum Eagle's medium (MEM, Gibco) supplemented with 10% fetal bovine serum (FBS, Gibco) and 1% penicillin (100 U/ml) or streptomycin (100 µg/mL) (Gibco). The cells were incubated in a 5% CO₂ incubator at 37 °C. Cells were stimulated with 1 µg/mL LPS (*E. coli*, Sigma Aldrich) or 10 ng/mL IL-4 (214–14, Peprotech) and 10 ng/mL IL-13 (210–13, Peprotech) in the presence of MGO or not for indicated time. Unless otherwise specified, the concentration of MGO was 200 µM.

2.4. Real-time PCR

Total RNAs from cultured cells were extracted and purified with RNA Easy Fast Tissue/Cell Kit (TIANGEN Cat# DP451), followed by reverse transcription using PrimeScript™ RT reagent Kit with gDNA Eraser (Takara Cat# RR047A). Real-time PCR was performed on a Bio-RadCFX96™ using ChamQ SYBR qPCR Master Mix (Vazyme Cat# Q321-02); β-actin was used as endogenous control. The primer sequences were obtained from published literature or PrimerBank and are listed in the Supplemental Materials (Table S1).

2.5. Western blot

Cells were lysed with cold RIPA buffer containing protease inhibitor cocktail (Beyotime, Beijing, China, P1005). Lysates were resolved by SDS-PAGE and proteins were transferred onto PVDF membranes (Millipore). After blocking with QuickBlock Western blocking buffer (Beyotime, P0252), the protein was detected with anti-mouse IκBα antibody (1:1000 dilution, Cell Signaling Technologies, 93726s) and anti-NRF2 antibody (1:1000 dilution, Cell Signaling Technologies, 12721s). The horseradish peroxidase-conjugated anti-rabbit IgG secondary antibody was used and Blots were developed on a Bio-rad Scanner.

2.6. Histochemistry and immunofluorescence

The spinal cords were fixed with 4% paraformaldehyde (PFA), embedded in paraffin, and cut into slices of 4 µm thickness. After deparaffinization and rehydration, hematoxylin-eosin (HE) and Luxol Fast Blue (LFB) staining were performed as previously described [19]. For fluorescence immunohistochemistry, the sections were incubated overnight with mouse monoclonal primary antibody against IBA1 (Servicebio, GB12105, 1:150) at 4 °C, followed by staining with a donkey anti-mouse IgG secondary antibody (Abcam, ab150108, 1:200). For fluorescence immunocytochemistry, the cells were harvested after gently repeated blowing, centrifuged at 1000 rpm, fixed with 4% PFA, permeabilized with 0.1% Triton ×100, and incubated with primary mouse monoclonal anti-MGO antibody (Abcam, ab243074, 1:200) at 4 °C overnight, followed by staining with donkey anti-mouse IgG secondary antibody (Abcam, ab150108, 1:200). All images were captured using Olympus BX51 or LEICA DMI8 microscope.

2.7. Cytometric bead-based immunoassay for multiplex cytokine profiling

Multiplex cytokine profiling of supernatants of stimulated BV2 cells was carried out using LEGENDplex™ Mouse Macrophage/Microglia Panel (13-plex) (Biolegend, Cat# No. 740846) was used according to the manufacturer's instructions. Data was acquired using a CytoFLEX S Flow Cytometer (Beckman Coulter) and analyzed using LEGENDplex™ data analysis software (Biolegend).

2.8. Supernatant H⁺ concentration was measurement

The supernatant H⁺ concentration was figured out by direct measuring the color change of phenol red (a traditional pH indicator dye) in the cell culture medium [20,21]. The standard samples with different H⁺ concentration (0, 0.3125, 0.625, 1.25, 2.5, 5 and 10 mM) were prepared by adding HCl into cell culture medium describe above. Then the absorption spectra of the standard samples and cell culture supernatant were taken using microplate reader (BioTek).

2.9. Glucose consumption assay

The glucose concentration in the supernatant was measured using glucometer (Sinocare Inc., Changsha, China) before and after cell culture. Glucose consumption was calculated by subtracting the remaining

glucose concentration after culture from the initial glucose concentration.

2.10. Spleen, lymph node and CNS-infiltrating leukocyte isolation

The spleen and lymph node were minced through a 70 μm cell filter to obtain a single-cell suspension. For the splenocytes, the red blood cell (RBC) lysis buffer was added to remove red blood cells, and CNS-infiltrating leukocytes were isolated through density gradient centrifugation. Briefly, after perfusing with PBS, the spinal cords were minced using a 70 μm cell filter and centrifuged at 1500 rpm for 5 min. The resulting pellet was collected and resuspended in 30% Percoll, layered on top of a 70% Percoll solution, and centrifuged at 800 g for 20 min. The intermediate cell layer was carefully harvested and extensively washed with cold PBS.

2.11. Flow cytometry

After extensive washing with a flow cytometry buffer (PBS with 2% FBS), the cells were stained with the following fluorescein-conjugated antibodies: CD3 (Alexa Fluor® 700, 17A2, BioLegend), CD4 (FITC, RM4-5, BioLegend; PE/Cyanine7, GK1.5, BioLegend), CD8 (PE, 53-6.7, BioLegend), CD11b (Brilliant Violet 421, M1/70, BioLegend), CD19 (PerCP/Cyanine 5.5, 6D5, BioLegend), CD25 (PE, PC61, BioLegend), CD45 (APC/Cyanine7, 30-F11, BioLegend), CD80 (PE, 16-10A1, BioLegend), CD86 (PerCP, GL-1, BioLegend), MHC II (APC, M5/114.15.2, BioLegend), PD-1 (APC, 29 F.1A12, BioLegend), CXCR5 (PE, L138D7, BioLegend), and Foxp3 (Alexa Fluor® 647, 150D, BioLegend). To detect Th1 and Th17 cells, mononuclear cells from the spleen and lymph nodes were stimulated with a Cell Stimulation Cocktail (eBioscience) for 4 h. After staining with live/dead fluorescent dye (Zombie Yellow Dye, BioLegend) and CD4 antibody (FITC, RM4-5, BioLegend), cells were fixed with 2% paraformaldehyde (PFA), washed with permeabilization buffer (eBioscience™), and counterstained with IL-17 (PECY5.5, eBio17B7, eBioscience™) and IFN- γ (PE, XMG1.2, BioLegend) antibodies.

For flow cytometry analysis, BV2 cells were harvested and washed with flow cytometry buffer, followed by staining with the following conjugated antibodies: CD80 (PE, 16-10A1, BioLegend), CD86 (PerCP, GL-1, BioLegend), MHC II (APC, M5/114.15.2, BioLegend), and GLUT1 (unconjugated, 21829-1-AP, Proteintech). Whereas, for unconjugated primary antibodies, the cells were stained with a fluorescein-conjugated secondary antibody, i.e., Goat Anti-Rabbit IgG H&L (Alexa Fluor® 488, Abcam). To detect intracellular proteins, the cells were fixed with 2% PFA, washed with permeabilization buffer (eBioscience), and stained with iNOS (PE/Cyanine7, CXNFT, eBioscience), Arg-1 (Alexa Fluor 488, AlexF5, eBioscience), or NRF2 (unconjugated, 16396-1-AP, Proteintech).

For intracellular MGO detection, cells were resuspended in the culture medium, stained with a living-cell fluorescent probe for MGO for 30 min at 37 °C, and detected using flow cytometry as described previously [22]. All data were analyzed using FlowJo 10.4 software.

2.12. Detection of mitochondrial membrane potential by JC-1

BV2 cells were seeded in a 6-well plate, and cell induction and drug intervention were performed as described above. The JC-1 fluorescent probe (Beyotime Cat# C2006) was assembled according to the manufacturer's instructions. Data were collected using flow cytometry.

2.13. Transwell migration assays

To assess lymphocyte migration *in vitro*, BV2 cells were seeded in the lower chamber and treated with LPS, LPS plus MGO, or the vehicle alone for 12 h. Following three thorough washes with PBS, a fresh culture medium was added to the chamber, and splenocytes were introduced to

the upper chamber (4 μm pore size; BD Falcon). After 12 h of co-culture, the cells in the lower chamber were harvested and stained with fluorescein-conjugated antibodies against CD3 (APC, 17A2, BioLegend) and CD4 (FITC, RM4-5, BioLegend). The stained cells were quantified using flow cytometry.

2.14. RNA sequence and data analysis

BV2 mouse microglia cells were stimulated with LPS in the presence of 200 μM MGO. After 24 h, cells were harvested and washed once with PBS before being lysed in TRIzol for 5 min at room temperature and frozen at -80 °C. The samples were sent to Novogene (Novogene.com) for library preparation and sequencing. Raw data (raw reads) in fastq format were first processed through in-house Perl scripts into low-quality reads. After mapping to the reference genome by Hisat2 (v2.0.5), FPKM was calculated based on the read count and length of each gene. In addition, differential expression analysis of the two groups was performed using the DESeq2 R package (version 1.20.0). To control the false discovery rate, *p*-values were adjusted using Benjamini and Hochberg's approach, with $\text{padj} \leq 0.05$ and $|\log_2(\text{fold change})| \geq 1$ considered statistically significant. Gene Ontology (GO) enrichment analysis of differentially expressed genes was performed using the clusterProfiler R package (3.8.1).

2.15. Small interfering RNA (siRNA) and plasmid transfection

NRF2 siRNA (si-NRF2, sense, 5'-UUGGGAUUCACGCAUAGGAGCA-CUG-3'; antisense, 5'-CAGUGCUCUAUGCGGAAUCCCAA-3') [23] and negative control (NC) siRNA were purchased from Genomeditech. $\text{I}\kappa\text{B}\zeta$ -overexpression and control plasmids were purchased from Genomeditech. The luciferase reporter plasmid ($\text{I}\kappa\text{B}\zeta$ -promoter-Luc), which contains an approximately 2 kb upstream region of the $\text{I}\kappa\text{B}\zeta$ -gene TSS followed by firefly luciferase, as well as the internal control reporter plasmid expressing Renilla luciferase (Renilla-Luc), were purchased from Genomeditech. BV2 cells were transfected with siRNA and the specified plasmids using electroporation, following the manufacturer's instructions (BEX CUY21EDIT II). The transfection efficiency was assessed using real-time PCR. After 24 h of transfection, BV2 cells were stimulated with 1 $\mu\text{g}/\text{mL}$ LPS \pm 200 μM MGO.

2.16. Luciferase reporter assays

Luciferase reporter assays were performed as follows: BV2 cells were transfected with the specified expression plasmids together with the luciferase reporter plasmid (promoter-Luc), and the internal control plasmid (Renilla-Luc) by electroporation. At 24 h after treatment, the cells were lysed; the luciferase activity was measured using the Dual-luciferase Reporter System (Vazyme). The luciferase activity was normalized to the Renilla luciferase activity of the internal control reporter.

2.17. Chromatin immunoprecipitation (ChIP) and qPCR

ChIP was performed using a Pierce Agarose ChIP kit (Thermo Scientific) according to the manufacturer's instructions. BV2 cells were seeded in 75 cm^2 plates and treated as previously described. After washing with cold PBS, BV2 cells were fixed with 1% (w/v) formaldehyde, quenched with glycine, incubated with lysis buffer, and centrifuged to obtain nuclear pellets. The nuclei were subsequently digested with micrococcal nucleases to generate chromatin fragments. After reserving 10% of the digested chromatin as the input, the remaining samples were incubated with rabbit *anti*-NRF2 monoclonal antibody (Cell Signaling Technology, D1Z9C) or rabbit IgG and retrieved with protein A/G agarose beads. The samples were then incubated at 65 °C for 40 min and digested with proteinase K. The DNAs were recovered using a column-based isolating method, and a qPCR analysis was

performed using the following primers: forward: 5'-TGCACAA-CACTGAAGGGTT-3,' reverse: 5'-CCAATAGACAGCGGGTGT-3.' The values obtained from the immunoprecipitated samples were normalized to those of the input DNA.

2.18. Statistical analysis

All data were analyzed using appropriate tests, including Student's *t*-test, one-way ANOVA, or two-way ANOVA, as applicable. The results are presented as mean values with standard error of the mean (SEM). Statistical significance was considered at $p < 0.05$. GraphPad Prism version 9 was used for data analysis.

3. Results

3.1. MGO was accumulated in multiple immune cells after stimulation

Boosted glucose uptake and flux through glycolysis are some of the most common metabolic reprogramming processes in immune cells after activation. In addition to supporting the energy and biosynthetic

demands of proliferation, glycolysis also leads to the generation of versatile metabolites, such as MGO (Figure s1). Indeed, it has been reported that MGO was significantly increased in polarized macrophages and the spinal cord of EAE mice [15,24]. In this study, by using a living-cell fluorescent probe for MGO, kindly provided by Wang et al. [22], we found that the intracellular levels of MGO were remarkably upregulated in LPS-stimulated microglial cell lines (Fig. 1a). MGO is a potent glycation agent that reacts with amino acids to form MGO-modified proteins (MGO-p) [10]; thus, intracellular MGO-p levels can serve as a proxy for MGO production. In line with the increased intracellular MGO levels in activated immune cells, intracellular MGO-p levels in BV2 cells were considerably elevated after activation with LPS, as illustrated by immunofluorescence (Fig. 1b).

Similarly, CD4⁺ and CD8⁺ lymphocytes activated with anti-CD3 and CD28 antibodies also showed accumulation of intracellular MGO as well as increased intracellular MGO-p (Fig. 1c and d, respectively). Interestingly, we found that Th1 (CD4+IFN- γ +) and Th17 (CD4+IL-17+) cells contained more intracellular MGO-p than non-Th1 (CD4+IFN- γ -) and non-Th17 (CD4+IL-17-) cells (Fig. 1e and f). However, there was no difference between Treg (CD4+Foxp3+) and non-Treg (CD4+Foxp3-)

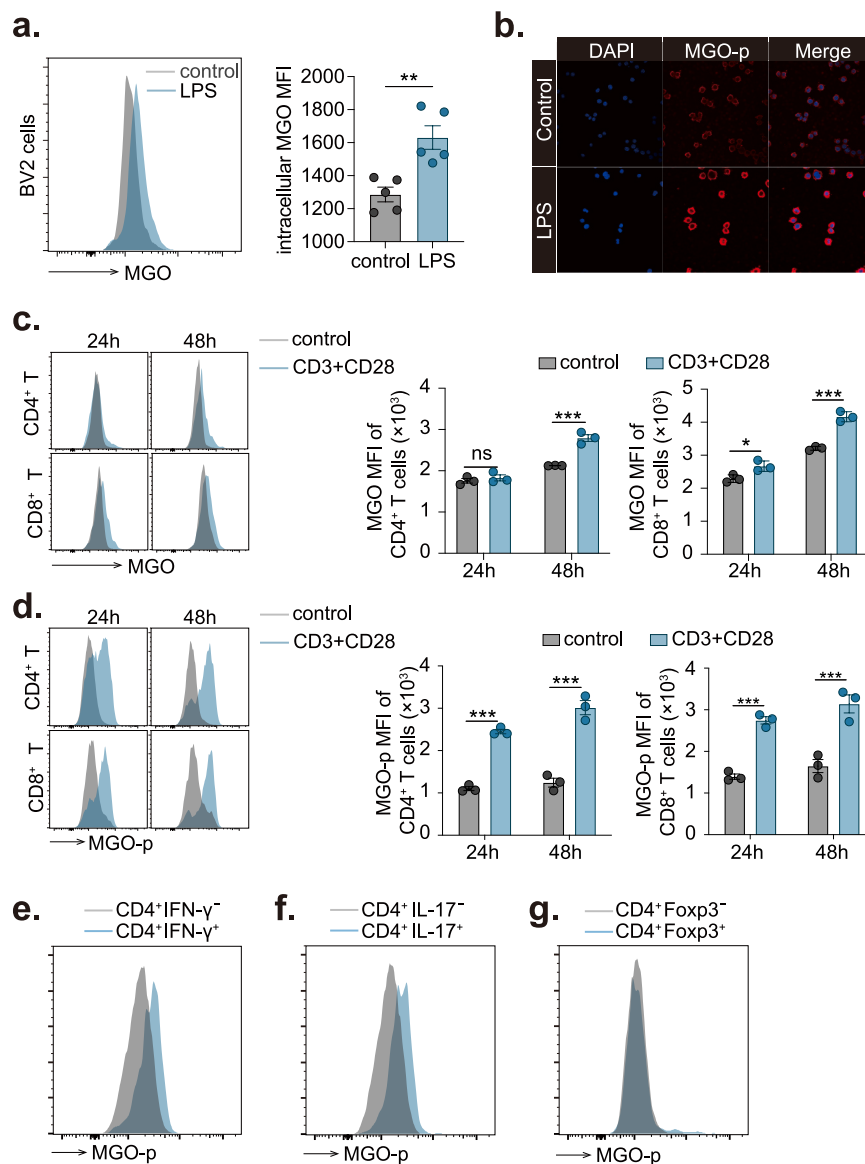


Fig. 1. MGOs are accumulated in activated immune cells.

(a) BV2 cells were stimulated with LPS (1 $\mu\text{g}/\text{mL}$) for 24 h. Intracellular MGO level was assessed using a fluorescent probe and detected through flow cytometry. (b) Immunofluorescent stain for intracellular MGO-modified proteins (MGO-p) in BV2 cells stimulated with LPS (1 $\mu\text{g}/\text{mL}$) for 24 h. (c) Mouse splenic CD3⁺ T cells were isolated and stimulated with anti-CD3 (1 $\mu\text{g}/\text{mL}$) and anti-CD28 (1 $\mu\text{g}/\text{mL}$) antibodies for the indicated time. Intracellular MGO levels were determined using a fluorescent probe and analyzed by flow cytometry. (d) Mouse splenic CD3⁺ T cells were isolated and stimulated with anti-CD3 (1 $\mu\text{g}/\text{mL}$) and anti-CD28 (1 $\mu\text{g}/\text{mL}$) antibodies for the indicated time. Intracellular MGO-p were measured using flow cytometry. (e) Flow cytometry analysis of intracellular MGO-p in Th1 (CD4+IFN- γ), non-Th1 (CD4+IFN- γ -), Th17 (CD4+IL-17+), non-Th17 (CD4+IL-17-), Treg (CD4+Foxp3+), and non-Treg (CD4+Foxp3-) cells. * $p < 0.05$; ** $p < 0.01$; *** $p < 0.001$. *Ns*, not significant. Three independent experiments were performed.

cells (Fig. 1g). These results were easy to interpret because Treg cells predominantly rely on mitochondrial OXPHOS, whereas Th1 and Th17 cells exhibit high glycolysis levels and consequently produce more MGOs. Overall, MGO accumulation is a common feature of activated immune cells that engage in enhanced glycolysis, and the increased MGO levels in the spinal cords of EAE mice may be attributed to the collective action of multiple immune cells.

3.2. MGO diminished CNS inflammation in EAE mice

To directly assess the role of MGO in the pathogenesis of EAE, C57BL/6 J mice were induced using EAE models and treated with MGO at 10 days after the immunization (Fig. 2a). Surprisingly, oral administration of 500 mg/kg MGO (dissolved in distilled water) twice daily ameliorated the clinical symptoms of EAE mice and alleviated the associated body weight loss (Fig. 2b). Concordantly, spinal cords from MGO-treated mice exhibited less inflammatory cell infiltration and demyelination in white matter, as illustrated by HE and LFB staining (Fig. 2c). Likewise, immunofluorescence staining showed fewer microglial cells in the lesion tissues of MGO-treated mice (Fig. 2d). However, neither the proportion nor the number of helper T cell subtypes, including Th1 (CD4+IFN- γ +), Th17 (CD4+IL-17+), and Tregs (CD4⁺CD25⁺Foxp3⁺), in the spleen and lymph nodes was statistically different between the two groups (Fig. S2). These results indicate that MGO might diminish EAE progression by targeting immune cells in the central nervous system but not peripheral immune organs. Flow cytometry analysis revealed fewer CD3⁺ T lymphocytes, CD4⁺ helper T cells, CD8⁺ cytotoxic T cells, and CD19⁺ B lymphocytes in the spinal cord of MGO-treated EAE mice (Fig. 2e and f). Furthermore, Th1 and Th17 cells were decreased in the CNS after MGO treatment (Fig. 2g), and no significant difference in the number of microglial cells between control and MGO-treated mice was observed (Fig. 2h). Additionally, the activation of microglial cells was gradually inhibited by MGO as the expressions of CD80, CD86, and MHC II in microglial cells were down-regulated after MGO treatment (Fig. 2i).

3.3. MGO modulated microglia polarization *in vitro*

Microglia, the main immune cells of the CNS, play a critical role as resident immunocompetent cells in the pathogenesis of MS/EAE. Like macrophages, microglial cells are highly adaptable to various micro-environmental clues. Based on their phenotypes and functions, microglial cells are traditionally categorized into M1 and M2 subtypes, which can be induced by LPS or IL-4 plus IL-13, respectively. To determine whether MGO modulates microglial cell polarization, BV2 cells were treated with MGO under different polarization conditions. Importantly, treatment with MGO did not significantly change the BV2 cell morphology or increase the cell apoptosis rate (Figs. S3a and S3b), thus, indicating that this treatment was well tolerated by BV2 cells *in vitro*. However, the treatment of BV2 cells with MGO resulted in a dose-dependent reduction in LPS-induced M1 polarization, as shown by the decreased inducible nitric oxide synthase (iNOS) expression observed through flow cytometry (Fig. 3a). In contrast, MGO did not significantly interfere with M2 polarization (Fig. 3b), indicating that MGO could modulate the balance between M1 and M2 polarization. To investigate this hypothesis, BV2 cells were cultured in media supplemented with LPS, IL-4, and IL-13 and simultaneously polarized to the M1 and M2 phenotypes (Fig. S3c). Consistent with our hypothesis, treatment with MGO upregulated the ratio of M2 to M1 phenotypes in BV2 cells (Fig. S3c). Further real-time PCR and flow cytometry analysis illustrated that the inflammation-relative genes, such as IL-1 β and IL-6, were down-regulated after MGO treatment (Fig. 3c to e). However, the expression levels of TNF- α were not different between the control and MGO-treated BV2 cells, which was confirmed by flow cytometry and real-time PCR (Fig. 3f).

To address the effects of MGO on cytokine production in BV2 cells,

we performed multiplex cytokine profiling of cell culture supernatants using a cytometric bead-based immunoassay. The pro-inflammatory cytokines such as IL-1 β , IL-6, IL-12, and IL-18 were markedly inhibited by MGO treatment (Fig. 3g). In addition, the levels of traditional anti-inflammatory cytokines, such as IL-10, decreased after MGO incubation.

3.4. MGO inhibited the capacity of microglia cells to recruit and activate lymphocytes

Overactive microglia play a critical role in EAE pathogenesis. First, chemokines secreted by microglial cells are responsible for the recruitment of autoreactive T lymphocytes to the CNS. Additionally, microglial cells activate autoreactive T lymphocytes by presenting autoantigens and producing inflammatory cytokines. Interestingly, in this study, MGO suppressed the antigen presentation capacity of microglial cells by inhibiting the expressions of CD80, CD86, and MHC II (Fig. 4a and b), which was consistent with the *in vivo* observations (Fig. 2i). However, the expressions of CD25 and ICOS in lymphocytes were markedly upregulated in LPS-stimulated BV2 cells compared to that in inactivated BV2 cells (Fig. 4c and d). Moreover, as expected, MGO diminished the activation effects of M1-polarized BV2 cells on lymphocytes (Fig. 4c and d).

Since MGO can also repress the secretion of chemokines such as CXCL2, CCL7, and CCL12 from BV2 cells (Fig. 4e), we analyzed the influence of MGO on the ability of BV2 cells to recruit inflammatory cells using a transwell assay. To exclude the direct effects of MGO on splenocytes, activated BV2 cells were pre-conditioned with MGO for 12 h and washed extensively with PBS before being co-cultured with splenocytes. As shown in Fig. 4f, the MGO-conditioned BV2 cells were less capable of recruiting T lymphocytes. This is consistent with the *in vivo* observations, in which MGO-treated mice showed less inflammatory cell infiltration in the spinal cord (Fig. 2f).

3.5. MGO suppressed microglia cell glycolysis by decreasing GLUT1 expression

Metabolites can form positive or negative autoregulatory feedback on metabolic pathways. Thus, as a nonenzymatic byproduct of the glycolytic pathway, it would be interesting to consider whether MGO could affect the glycolytic pathway. Extracellular acidification is a commonly used index for monitoring glycolysis. Phenol red is often used as a pH indicator in the culture medium: its color gradually changes from yellow to red over the pH range of 6.6–8.0. We measured the absorption spectra of the complete culture medium with different concentrations of hydrochloric acid. As shown in Fig. 5a, there were two absorption peaks for the complete culture medium, corresponding to 415 and 560 nm. With an increase in the hydrochloric acid concentration, the absorbance at 415 nm increased, whereas that of 560 nm decreased. The ratios between the absorbance at 415 and 560 nm showed a linear correlation with the hydrochloric acid concentration (Fig. 5a). These results suggest that spectrophotometry can serve as a convenient and efficient approach for monitoring extracellular acidification. Consequently, we applied this method to detect acidification of the culture medium and found that LPS-activated BV2 cells produced a significant amount of acid in the culture medium compared to BV2 cells in their resting state (Fig. 5b). Interestingly, the addition of MGO reversed the activation-induced acid production in BV2 cells (Fig. 5b).

Furthermore, in line with abrogated glycolysis, the glucose consumption rate of BV2 cells was also diminished by MGO treatment (Fig. 5c). Glucose transporters (GLUTs) accomplish the movement of glucose from the extracellular space into cells. Therefore, targeting GLUTs is a key metabolic checkpoint in several immune cells, including T lymphocytes and microglia cells [25–27]. The GLUT family comprises at least 14 members with distinct tissue distributions. Specifically, GLUT1 is essential for glucose uptake by microglia cells [25], and immunofluorescence staining revealed that GLUT1 expression was

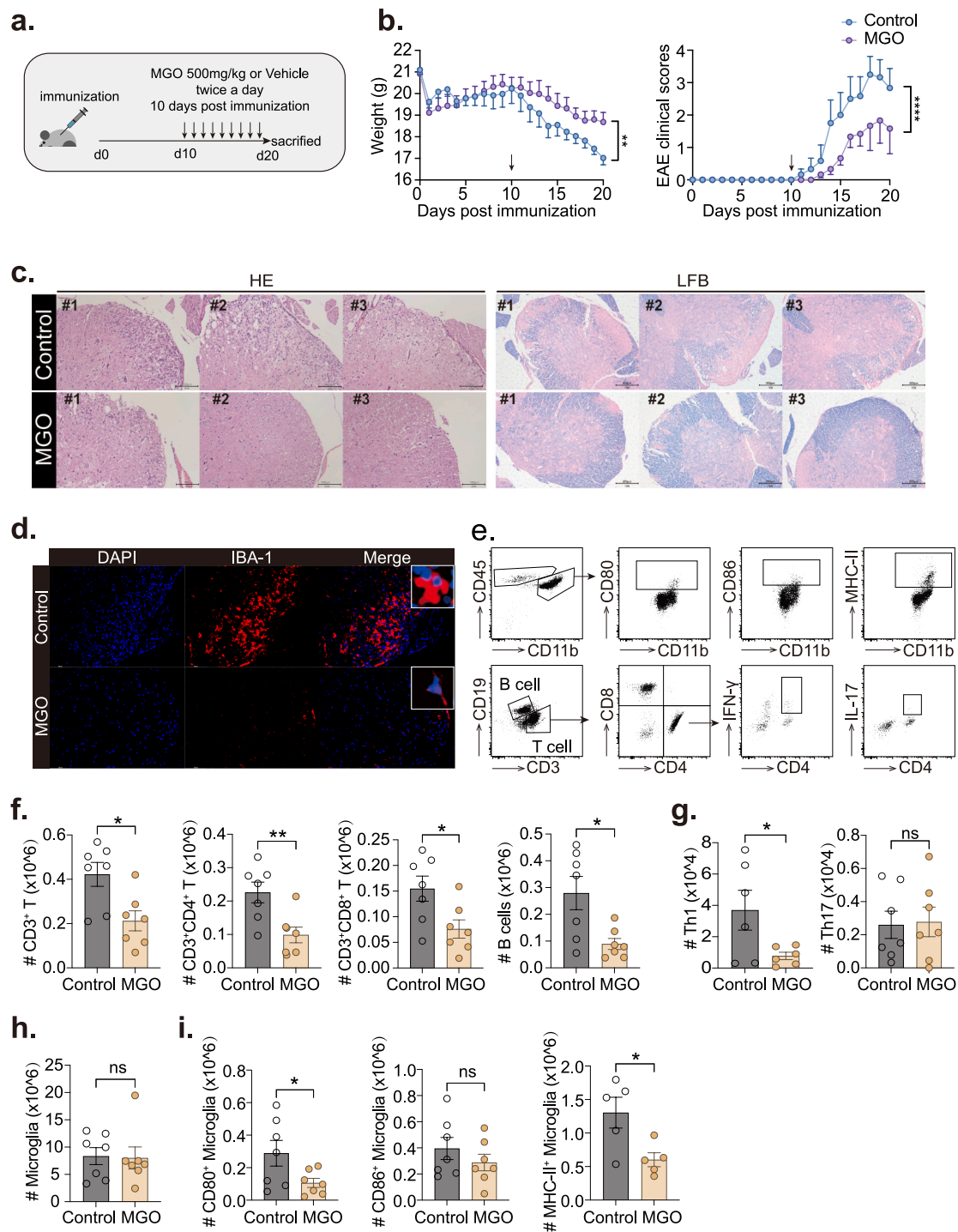


Fig. 2. MGO treatment diminishes experimental autoimmune encephalomyelitis.

(a) Schematic of EAE immunization and treatment. EAE mice were treated with 500 mg/kg MGO (dissolved in water) or equal volume of vehicle (water) twice a day at 10 days post immunization. (b) Mean clinical scores and body weights of EAE in MGO-treated (MGO) mice or controls. (c) Cross-sectional images of the spinal cord stained with hematoxylin and eosin (HE) and Luxol Fast Blue (LFB). (d) Immunofluorescent staining for IBA-1 in the spinal cord. (e) Gating strategy for immune cells in the spinal cords of EAE mice. (f) Quantification of CD3+ T cells, CD3+CD4+ T cells, CD3+CD8+ T cells, and B cells in the spinal cords of EAE mice. (g) Quantification of Th1 (CD4+IFN- γ +) and Th17 (CD4+IL-17+) cells in the spinal cords of EAE mice. (h) Quantification of microglia cells (CD45^{low}CD11b+) in the spinal cords of EAE mice. (i) Quantification of CD80, CD86 or MHC II-positive microglia cells (CD45^{low}CD11b+) in the spinal cords of EAE mice. Pooled data for two independent experiments. N = 6 for each group. * p < 0.05; ** p < 0.01; *** p < 0.001, **** p < 0.0001. Ns, not significant. (For interpretation of the references to color in this figure legend, the reader is referred to the Web version of this article.)

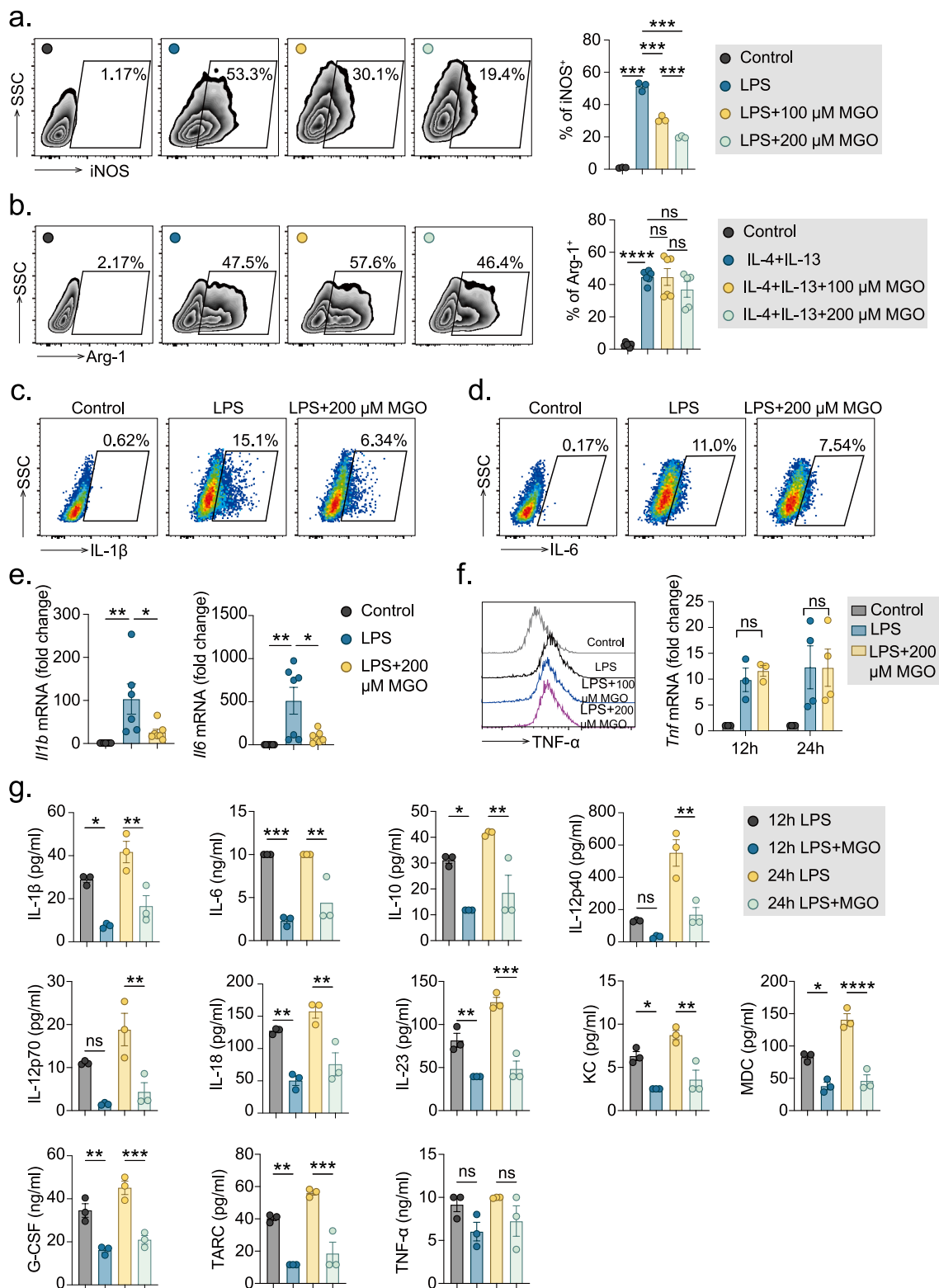


Fig. 3. MGO modulates microglia polarization *in vitro*.

(a) Flow cytometry analysis of iNOS expression in BV2 cells treated with LPS and different concentrations of MGO for 24 h. (b) BV2 cells were stimulated with IL-4 plus IL-13 in the presence or absence of MGO for 24 h, and the expression of Arg-1 was analyzed by flow cytometry. (c and d) Flow cytometry analysis of IL-1β and IL-6 expressions in BV2 cells treated with LPS ± 200 μM MGO for 24 h. (e) Real-time PCR analysis of IL-1β and IL-6 expressions in BV2 cells treated with LPS ± 200 μM MGO for 24 h. (f) Flow cytometry and real-time PCR analysis of TNF-α expression in BV2 cells treated with LPS ± 200 μM MGO for 24 h. (g) BV2 cells treated with LPS and 200 μM MGO for 12 or 24 h, multiplex cytokine profiling of supernatants was analyzed by cytometric bead-based immunoassay. **p* < 0.05; ***p* < 0.01; ****p* < 0.001. Ns, not significant. Three independent experiments were performed.

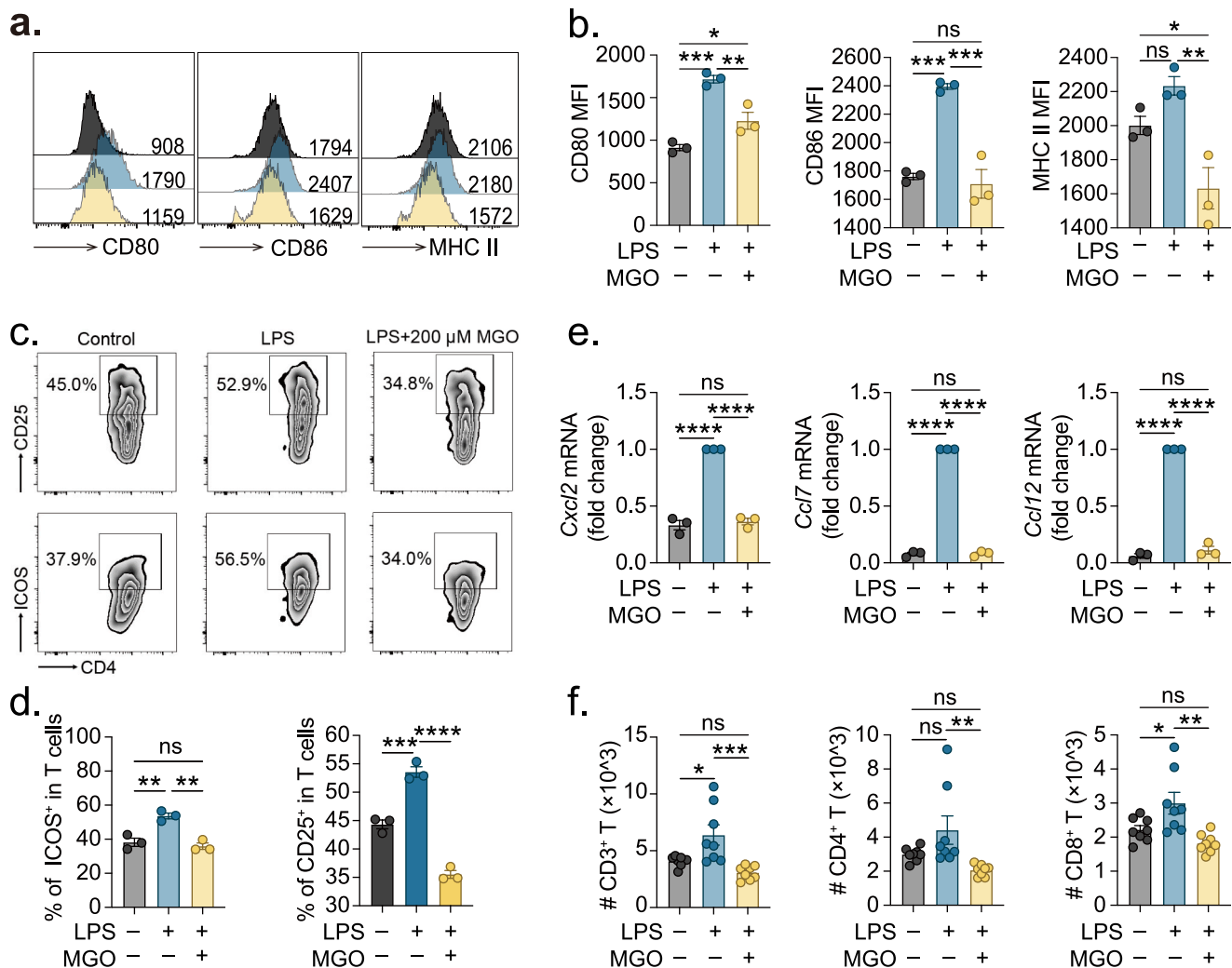


Fig. 4. MGO inhibits the capacity of microglia cells to recruit and activate lymphocytes.

BV2 cells were stimulated with 1 μg/mL LPS ±200 μM MGO for 12 h. (a and b) The expressions of CD80, CD86, and MHC II on the surface of BV2 cells were measured using flow cytometry. (c and d) BV2 cells were washed three times with PBS and co-cultured with purified mouse splenic T lymphocytes at a ratio of 1:10. After 3 d, the cells were harvested, stained with antibodies against CD4, CD25, and ICOS, and analyzed using flow cytometry. (e) Expressions of CXCL2, CCL7, and CCL12 were detected using real-time PCR. (f) A transwell assay was applied to lymphocytes co-cultured with LPS or LPS plus MGO-stimulated BV2 cells, and cell numbers were counted by flow cytometry. **p* < 0.05; ***p* < 0.01; ****p* < 0.001, *****p* < 0.0001. Ns, not significant. Three independent experiments were performed.

reduced in MGO-conditioned BV2 cells (Fig. 5d), as confirmed by flow cytometry (Fig. 5e). However, MGO did not interfere with the oxidative phosphorylation of BV2 cells, as equal levels of mitochondrial membrane potential were observed in the control and MGO groups (Fig. 5f). These results suggest that MGO inhibits glycolysis in M1-polarized BV2 cells by decreasing GLUT1 expressions.

3.6. MGO exerts anti-inflammatory effects on microglia cells by suppressing *IκBζ* transcription

To obtain an overall perspective on the immunomodulatory effects of MGO, we performed mRNA sequencing of BV2 cells under M1-polarization conditions. In total, 235 genes were differentially expressed after treatment with MGO, of which 111 were upregulated and 125 were downregulated (Fig. 6a). GO classification and enrichment analyses revealed that many genes involved in inflammatory response were differentially expressed (Fig. 6b). Except for a few genes, we observed a general decrease in the expression of inflammatory response-related genes in response to MGO treatment, including *Il1a*, *Il-*

1b, *Il-6*, and *Il12b* (Fig. 6c).

To address the mechanisms of anti-inflammatory effects of MGO, we perform gene set enrichment analysis (GSEA) of RNA-seq data described above and found that the Toll-like receptor and NF-κB pathways were remarkably suppressed after treatment with MGO (Fig. 6d and e). NF-κB is a transcriptional factor that controls the expression of varieties of cytokines and other immune regulators. According to kinetics, the NF-κB target genes can be categorized into two groups, rapid or delayed expression. The rapid-expressed genes include TNF-α, while the delayed-expressed genes include IL-1β, IL-6, IL-12, CCL2, and M-CSF. One known factor that influences the regulation of delayed-expressed genes is *IκBζ* [28,29]. Interestingly, treatment with MGO considerably diminished delayed-expressed genes in the NF-κB pathway, such as IL-1β, IL-6, and IL-12 (Fig. 6c), but not rapid-expressed genes (Fig. 3f), which indicated MGO might influence NF-κB pathway by targeting *IκBζ*. To test our hypothesis, the expression levels of *IκBζ* were determined using RT-PCR and western blot. Indeed, expressions of *IκBζ* were decreased upon MGO treatment both at mRNA and protein levels (Fig. 6f), and as expected, the overexpression of *IκBζ* by transfection with *IκBζ*-overexpression

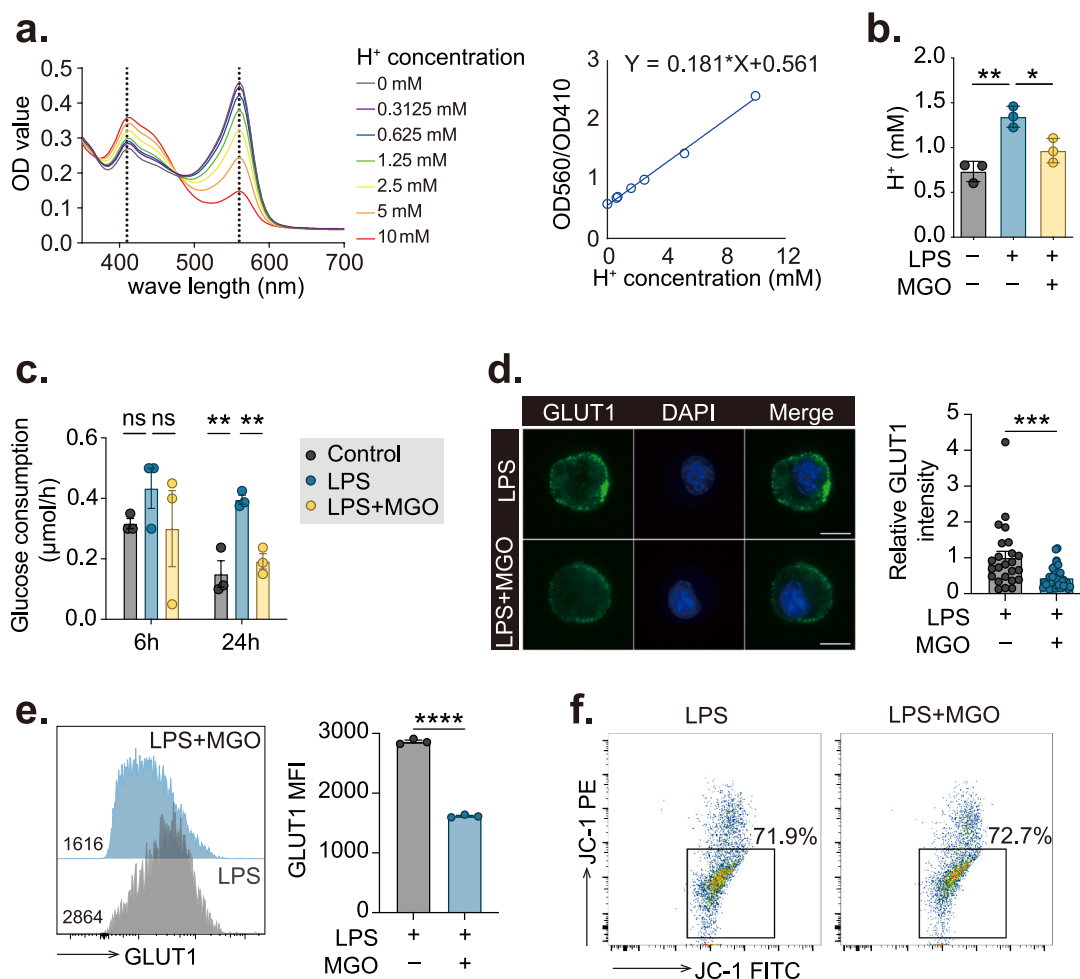


Fig. 5. MGO suppresses microglia cell glycolysis by decreasing GLUT1 expression.

(a) The absorption spectrum of the complete culture medium with different concentrations of hydrochloric acid (left) and correlation analysis of ratios of absorbance at 415–560 nm with the concentrations of hydrochloric acid (right). (b) Acid concentration in the supernatant of BV2 cells treated with 1 μg/mL LPS ± 200 μM MGO for 24 h. (c) Glucose consumption of BV2 cells treated with 1 μg/mL LPS ± 200 μM MGO was measured after 6- and 24-h incubation. (d) Immunofluorescent stain of GLUT1 on BV2 cells after treatment with LPS ± 200 μM MGO for 24 h. (e) Flow cytometry analysis of GLUT1 on the surface of BV2 cells treated with LPS ± 200 μM MGO for 24 h. (f) BV2 cells were stimulated with 1 μg/mL LPS ± 200 μM MGO for 24 h. Mitochondrial membrane potentials were addressed using JC-1 fluorescent probe and analyzed by flow cytometry. Three independent experiments were performed. **p* < 0.05; ***p* < 0.01; ****p* < 0.001. Ns, not significant.

plasmid reversed the inhibitory effects of MGO on IL-1β and iNOS expressions (Fig. 6g), indicating that IκBζ was responsible for the anti-inflammatory effects of MGO.

Previous studies have illustrated that mRNA stability plays a critical role in the regulation of IκBζ expression [30]. However, in this study, MGO did not affect the degradation of IκBζ mRNA, as the mRNA decayed with the same kinetics in both control and MGO-treated BV2 cells after terminating the transcription of IκBζ mRNA with doxycycline (dox) (Fig. 6h). In addition, the transcription level of MCP1P, which was responsible for the degradation of IκBζ mRNA, was also not changed after MGO treatment (Fig. 6i). Using the luciferase reporter construct, which contains the promoter (-1–2000 bp) of IκBζ followed by firefly luciferase, we found that MGO suppressed luciferase activity stimulated by LPS (Fig. 6j). These results indicated that MGO inhibited IκBζ expression by suppressing its transcriptional activity.

3.7. The anti-inflammatory effects of MGO on microglia cells were depended on NRF2 pathway

NRF2 is a master transcriptional regulator of genes whose products protect the cells against oxidative stress. NRF2 exhibits both antioxidant

and anti-inflammatory properties. During oxidative stress, NRF2 is activated, translocated to the nucleus, upregulating several antioxidant genes, including heme oxygenase-1 (HO-1), NQO-1, GCLM, and GCLC. Previous studies have revealed that MGO activates the NRF2 signaling pathway [31], and in this study, treatment with MGO remarkably enhanced the expression of HO-1, NQO-1, GCLM, and GCLC (Fig. 7a). Immunofluorescence staining revealed that nuclear accumulation of NRF2 in microglial cells increased after MGO treatment (Fig. 7b).

To assess the requirement of NRF2 for the immunosuppressive effects of MGO, microglial cells were transfected with NRF2-siRNA or control siRNA prior to LPS and MGO stimulation. As illustrated in Fig. 7c, transfection with NRF2-siRNA efficiently blocked NRF2 transcription. However, interference with this pathway reversed the MGO-stimulated HO-1, NQO-1, GCLM, and GCLC upregulation (Fig. S4a). Likewise, siRNA-mediated knockdown of NRF2 in BV2 cells reversed the inhibitory effects of MGO on inflammatory cytokine transcription and iNOS expression (Fig. 7d and e). Interestingly, the supplementation of the culture medium with GSH, a key antioxidant that scavenges free oxygen radicals and suppresses the NRF2 pathway, reversed the MGO-induced upregulation of HO-1, NQO-1, GCLM, and GCLC (Fig. S4b). Additionally, MGO did not inhibit IL-1β expression in the presence of exogenous

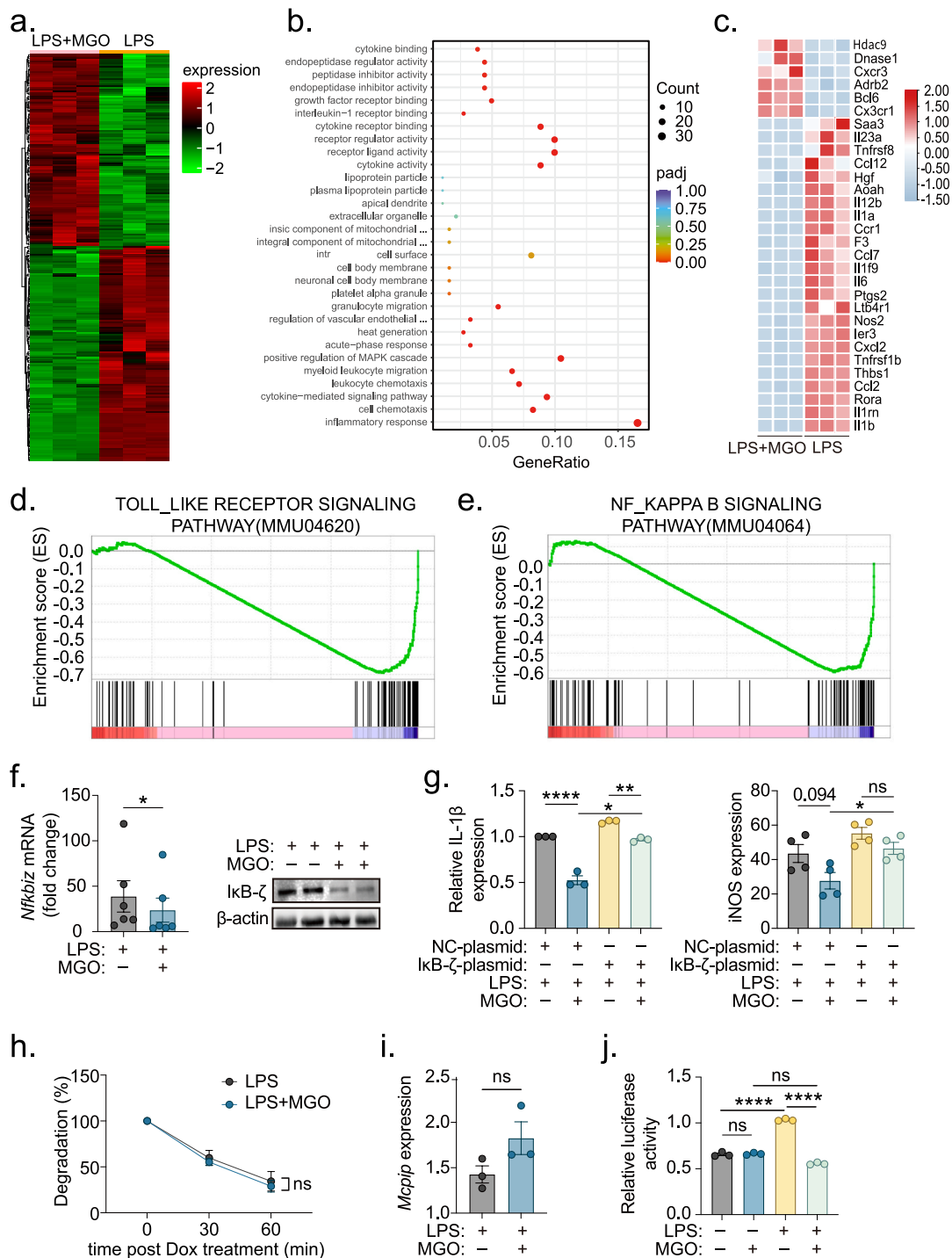


Fig. 6. MGO restrains pro-inflammatory cytokine production by suppressing IκBζ expression.

BV2 cells were stimulated with 1 μg/mL LPS and 200 μM MGO for 24 h. Gene expression was determined using RNA sequencing. (a) Heatmap depicting differentially expressed genes between LPS-stimulated and LPS plus MGO-conditioned BV2 cells. (b) GO analysis of differentially expressed genes between the two groups. (c) Heatmap depicting differentially expressed genes related to inflammatory responses. (d and e) GSEA of enriched Toll-like receptor and NF-κB signaling pathways. (f) Real-time PCR and western blot analysis of IκBζ (*Nfkbiz*) expression in BV2 cells stimulated with 1 μg/mL LPS and 200 μM MGO for 24 h. (g) BV2 cells were electroporated with IκBζ-expression plasmid (IκBζ-plasmid) or control plasmid (NC-plasmid) and stimulated by 1 μg/mL LPS ± 200 μM MGO for 24 h. Expression levels of IL-1β and iNOS were determined using flow cytometry. (h) BV2 cells were stimulated with 1 μg/mL LPS ± 200 μM MGO for 2 h and treated with doxycycline for the indicated time. The *Nfkbiz* (IκBζ) mRNAs were determined by real-time PCR. (i) BV2 cells were stimulated with 1 μg/mL LPS ± 200 μM MGO for 24 h, and the expression of *Mcpip* was analyzed by real-time PCR. (j) BV2 cells were electroporated with firefly luciferase-reporter plasmid (IκBζ-promotor-Luc) and the internal control plasmid (Renilla-Luc) and stimulated with 1 μg/mL LPS ± 200 μM MGO for 24 h. Firefly luciferase activity was determined and normalized to the Renilla luciferase activity. Three independent experiments were performed. * $p < 0.05$; ** $p < 0.01$; *** $p < 0.001$. Ns, not significant.

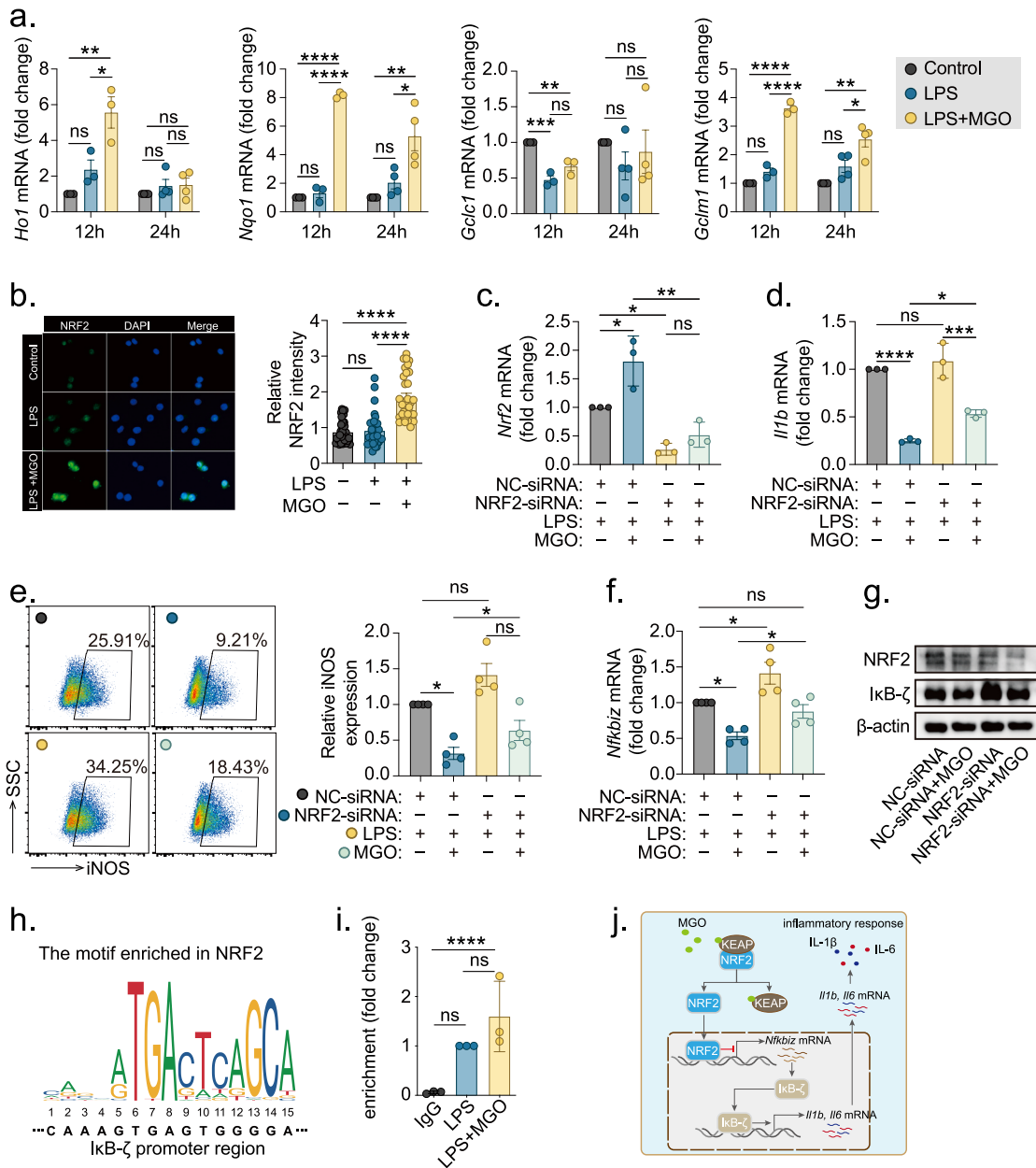


Fig. 7. MGO suppresses pro-inflammatory cytokine production through the NRF2 pathway.

(a) Real-time PCR analysis of *Ho1*, *Nqo1*, *Gclc*, and *Gclm* of BV2 cells stimulated with 1 $\mu\text{g}/\text{mL}$ LPS \pm 200 μM MGO for 12 and 24 h. (b) Immunofluorescent stain of NRF2 in BV2 cells after treatment with LPS \pm 200 μM MGO for 24 h. (c) BV2 cells were electroporated with NRF2-siRNA or NC-siRNA and stimulated with 1 $\mu\text{g}/\text{mL}$ LPS \pm 200 μM MGO for 24 h. NRF2 knock-down efficiency after NRF2-siRNA electroporation detected by real-time PCR. (d) Expression of IL-1 β was addressed by real-time PCR. (e) Expressions of iNOS were determined by flow cytometry. (f and g) Expression of *IκBζ* was addressed by real-time PCR and Western blot. (h) Putative NRF2-binding site at *IκBζ* promoter predicted by JASPAR. (i) BV2 cells were stimulated with LPS \pm 200 μM MGO for 6 h, and ChIP assays were performed with antibodies against NRF2 or control rabbit IgG. The precipitated DNA containing the *IκBζ* promoter was assayed by quantitative real-time PCR with specific primers. (j) Schematic diagram showing the mechanism of action of MGO. Representative data from at least three independent experiments. * $p < 0.05$; ** $p < 0.01$; *** $p < 0.001$. Ns, not significant.

GSH (Fig. S4c). Taken together, these results indicate that MGO suppresses the inflammatory response by activating the NRF2 pathway.

NRF2 counteracts the inflammatory response at multiple layers. Based on the observation from the above experiments, we hypothesized that NRF2 could directly affect *IκBζ* expression at the transcription level. Indeed, suppressing NRF2 expression with NRF2-siRNA upregulated *IκBζ* expression at both the mRNA and protein levels (Fig. 7f and g). Using the JASPAR database, we identified several putative binding motifs in the promoter region of the *IκBζ* gene (Fig. 7h), and using the

Cistrome data browser, we found the NRF2-binding peaks at the promoter region of the *IκBζ* gene both in mice and humans (Figs. S5a and S5b). Besides, the chromatin immunoprecipitation (ChIP) assay confirmed that NRF2 is recruited to the promoter region of *IκBζ*, and this recruitment was enhanced after MGO treatment (Fig. 7i).

4. Discussion

Metabolic reprogramming is a crucial process in the activation and

differentiation of immune cells. These changes are not only important for meeting energy demands and generating biosynthetic precursors but also for the accumulation of metabolites that can function as signaling molecules and regulate immune reactions [32]. MGO is a highly reactive metabolite mainly generated from the glycolytic intermediates, GA3P and DHAP, through nonenzymatic allostereism [3]. Our results shows intracellular MGO level is increased in activated immune cells, such as microglia and lymphocytes. MGO acts as anti-inflammatory metabolite by modulating M1-polarization, inflammatory cytokine production and metabolic reprogramming of microglia cells and inhibits neuro-inflammation of EAE mice. Mechanically, we found that MGO activated NRF2 pathway and NRF2 could bind to the promoter of $\text{I}\kappa\text{B}\zeta$ gene and suppressed its transcription and subsequently pro-inflammatory cytokine production.

While MGO can be produced as a by-product of both amino acid and fatty acid metabolism, the glycolytic pathway represents the most important endogenous source of MGO [10]. It has been estimated that 0.1–0.4% of the glycolytic flux results in MGO production [10]. Thus, it is easy to interpreted that immune cells with higher glycolysis rate will produce larger amount of MGO. Indeed, accumulation of MGO might be a common feature of activated immune cells with enhanced glycolysis. These cells included LPS-activated microglial cells (Fig. 1a), macrophages [11], and activated CD4⁺ and CD8⁺ lymphocytes (Fig. 1b). Additionally, increased MGO levels have been observed in the serum of patients with RA and tissues of MS [15,16]. Serum MGO levels were positively correlated with the disease activity of RA [16]. Although whether the MGO is increased in patients with systemic lupus erythematosus (SLE) has not been determined yet, the advanced glycation end products, which can be formed from MGO, are indeed increased [33]. These results imply that MGO and its modified protein might act as the biomarker of inflammation. Nevertheless, many researches in the fields still deserve further exploration.

Extensive studies have revealed the immune regulation of metabolites generated from glycolysis pathway, TCA cycle and amino acid metabolism. Itaconate is one of the best examples of metabolic reprogramming which connects cell metabolism, oxidative and electrophilic stress responses and immune responses [34,35]. Upon inflammatory macrophage activation, itaconate is synthesized by diverting aconitate away from the TCA cycle, which in turn modulated macrophage metabolism and restrains macrophages inflammatory response [36]. The uncovered mechanisms of itaconate action include transcriptional regulation of activating transcription factor 3 (ATF3) signal pathway and protein modification regulation of KEAP1, inflammasome, JAK1 and TET2 [37–40]. Interestingly, as a by-product of glycolytic pathway, MGO shares several similarities with itaconate. Firstly, both of them are generated during the activation of LPS-stimulated macrophage [11,36]. Secondly, both exhibit direct antibacterial effects [11,41,42]. Thirdly, both can activate the NRF2 pathway by directly modifying Kelch-like ECH-associated protein (KEAP) and are potent antioxidants [31,43]. However, compared to the well-characterized “star molecular” itaconate, MGO is often overlooked. This might be because MGO is mainly generated through a nonenzymatic pathway and traditionally considered as a metabolic byproduct. However, accumulating evidence reveals the profound effects of MGO on multiple biological processes [31,44]. Our study demonstrated that MGO, similar to itaconate, reduced pro-inflammatory cytokines and restrained autoimmunity. These results indicated that MGO might be one of inherent negative-feedback immunometabolite employed by immune cells to limit excessive inflammation response.

It has been proposed that MGO is a relatively low-abundance metabolite with plasma concentration of around 50–300 nM and intracellular concentration of around 1–2 μM in healthy individuals [9,45,46]. Although the endogenous MGO is also upregulated in LPS-stimulated microglia cells, it remains to be determined whether endogenous MGO exerts similar anti-inflammatory effects. One concern is that the concentration of endogenous MGO might be far lower than

exogenous MGO used in our experiments. Due to its highly reactive electrophilic nature, approximately 99% of cellular MGO is reversibly bound to biopolymers and small-metabolite thiols, with only 1% of MGO remaining unbound [9,47]. The intracellular unbound MGO are typically in the low μM range, while the total (unbound + bound) MGO can reach up to 300 μM [10]. Importantly, as MG is highly reactive its half life is short in a biological environment and therefore, at the time and site of production, local concentrations may be significantly higher [48]. Indeed, works carried by Bollong et al. revealed that pharmacologically augmenting endogenous MGO generation could also activate KEAP-NRF2 signaling [31]. Another study also provide the evidence of immune-suppressive activity of endogenous MGO [49]. These results support the notion that endogenous MGO could act as immune-suppressive metabolite.

Due to its highly reactive electrophilic nature, post-translational modifications (PTMs) of proteins by MGO may be the primary mechanism through which MGO regulates diverse biological processes. Studies carried out by Gilligan et al. demonstrated that MGO-derived post-translational arginine modifications are abundant in histones, and their levels are comparable to those of other canonical Lys and Arg modifications. In addition, 28 site-specific histone modifications were identified, indicating the diversity of this type of PTM on histones [44]. Thus, these modifications were proposed to disrupt basal canonical histone PTMs by acetylation and ubiquitylation [44]. MGO can also form covalent modifications with the cysteine and arginine residues of KEAP1, leading to the dimerization of KEAP1 and activation of the NRF2 transcriptional program [31]. Consistent with these findings, our study demonstrated an activated NRF2 pathway in MGO-treated microglial cells. Additionally, A higher level of MGO-modified proteins was observed in activated microglia, activated lymphocytes, and Th1- or Th17-polarized helper T cells in our experiments. It will be attractive to fully reveal the types and roles of MGO-derived PTMs in these immune cells under both physiological and pathophysiological conditions.

The regulatory system of NRF2 activity is an attractive drug target because of its protective effects against CNS inflammatory diseases, including EAE. Oxidative species generated by activated microglia play critical roles in EAE progression [50,51]. Since the CNS is highly susceptible to ROS-induced damage [51], it has been shown that cultured oligodendrocytes and myelin-producing cells within the CNS degenerate upon exposure to chemically induced ROS [52,53]. Furthermore, several studies have also illustrated the anti-inflammatory properties of the NRF2 pathway in addition to its antioxidant function [54]. NRF2 counteracts the NF- κB -dependent inflammatory response through multiple layers. Since NRF2 upregulates numerous antioxidant genes, the elimination of ROS is considered the first layer of the molecular basis for NRF2-mediated anti-inflammation [55,56]. Moreover, NRF2 prevents the proteasome-dependent degradation of $\text{I}\kappa\text{B}\alpha$, which binds to and inhibits the nuclear translocation of NF- κB [55,57]. In addition, NRF2 can be recruited to the regulatory regions of pro-inflammatory cytokine genes, interfering with the activity of pro-inflammatory transcription factors and inhibiting pro-inflammatory transcription [58]. Notably, we found that NRF2 suppressed $\text{I}\kappa\text{B}\zeta$ expression as well as pro-inflammatory cytokine production. $\text{I}\kappa\text{B}\zeta$ is an atypical nuclear $\text{I}\kappa\text{B}$ protein and a selective co-activator of NF- κB target genes. $\text{I}\kappa\text{B}\zeta$ is responsible for the delayed expression of genes in the NF- κB signaling pathway, including IL-1 β , IL-6, IL-12, CCL2, and M-CSF. Both transcriptional activation and post-transcriptional mechanisms have been shown account for the regulation of $\text{I}\kappa\text{B}\zeta$ expression [28]. Our study showed that NRF2 binds to the promoter of the $\text{I}\kappa\text{B}\zeta$ gene, suppresses its transcription, and subsequently inhibits the inflammatory response. These results provides new insights into the mechanism through which NRF2 regulated $\text{I}\kappa\text{B}\zeta$ expression.

Our results also demonstrated that MGO acts as a metabolic regulator during the M1-polarization of BV2 cells. Indeed, MGO inhibited glycolysis in LPS-activated microglial cells, as shown by decreased acid production and glucose consumption after MGO treatment. It have been

demonstrated that enhanced glycolysis is a critical feature of microglial polarization and plays a critical role in regulating the immune response. GLUT1, highly expressed in microglia, is essential for glucose uptake and glycolysis maintenance. Pharmacologically blocking GLUT1 reprogrammed pro-inflammatory microglia from glycolytic to OXPHOS, suppressing microglial cell activation and pro-inflammatory cytokine production [25]. Our results demonstrated treatment with MGO diminished GLUT1 expression on microglial cell surfaces. These results are consistent with a previous report by Jandova et al. in which augmenting MGO production by genetically interfering with GLO-1 expression suppressed GLUT1 expression and glucose consumption in human tumor cells [59]. Although the precise molecular mechanism is complicated and still needs to be elucidated, our findings support the notion that MGO negatively regulates glycolysis in M1-polarized microglial cells by suppressing GLUT1 expression. Previous works demonstrated that MGO can directly bind to key enzymes involved in glycolysis, including glyceraldehyde-3-phosphate dehydrogenase (GAPDH) and pyruvate kinase M2 (PKM2) [60,61]. Whether MGO suppress microglia glycolysis through GAPDH and PKM2 is another interesting topics remain to be confirmed.

In conclusion, our study highlights that MGO is a potent compound that can inhibit CNS autoimmunity by influencing microglial cell polarization and restraining the inflammatory response through the NRF2-IκB ζ pathway. MGO is another example of metabolite which connects cell metabolism, oxidative and electrophilic stress responses and immune responses. Therefore, we believe that the MGO metabolic pathway may be a novel therapeutic target for the treatment of MS and other autoimmune diseases.

Data sharing statement

All data will be made available by the corresponding author upon reasonable request.

Ethical approval and consent to participate

All animal experiments were reviewed and approved by the Institutional Animal Care and Use Committee of the First Affiliated Hospital of Shandong First Medical University.

Consent for publication

All authors listed gave consent for publication.

Availability of data and materials

All data generated or analyzed in this study are included in the published article. All data will be made available from the corresponding author upon reasonable request.

Funding

This study was funded by the Natural Science Foundation of Shandong Province, China (ZR2021QH019), the National Natural Science Foundation of China (82101421, 82101487), and the Academic Promotion Program of Shandong First Medical University (2019QL013).

Authors' contributions

Chun-Lin Yang and Rui-Sheng Duan designed, analyzed, and provided overall guidance for the experiments. Shu-Li Wei designed, performed, and analyzed the experiments and wrote the manuscript. Ying Yang, Wei-Yue Si, Yang Zhou, Tao Li, and Tong Du performed the experiments. Peng Zhang, Xiao-Li Li, and Ruo-Nan Duan performed statistical analyses. All authors have read and approved the final manuscript.

Declaration of competing interest

The authors declare that they have no known competing financial interests or personal relationships that could have appeared to influence the work reported in this paper.

Data availability

Data will be made available on request.

Abbreviations

AGEs	advanced glycation end products
CCL:	C–C Motif Chemokine Ligand
CFA	complete Freund's adjuvant
CNS	central nervous system
CXCL:	C–X–C motif chemokine ligand
DHAP	dihydroxyacetone phosphate
EAE	experimental autoimmune encephalomyelitis
FBS	fetal bovine serum
GCLC	glutamate-cysteine ligase catalytic subunit
GCLM	glutamate-cysteine ligase modifier subunit
GLUT	glucose transporter
HE	Hematoxylin-Eosin
HIF-1 α	hypoxia-inducible factor 1 α
HO-1	heme oxygenase-1
KEAP1	Kelch-like ECH-associated protein 1
IFN- γ :	interferon γ
IL:	Interleukin
I κ B- α :	NF-kappa-B inhibitor alpha
iNOS	inducible nitric oxide synthase
LFB	Luxol Fast Blue
LPS	Lipopolysaccharide
MEM	minimum Eagle's medium
MGO	methylglyoxal
NF- κ B	nuclear factor-kappa B
NQO-1	NAD(P)H quinone dehydrogenase 1
NRF2	nuclear factor erythroid 2-related factor
OXPHOS	oxidative phosphorylation
PBS	phosphate buffer saline
PFA	paraformaldehyde
PTMs	post-translational modifications
ROS	reactive oxygen species
RT-PCR	Real-time PCR
siRNA	small interfering RNA
TCA	tricarboxylic acid

Appendix A. Supplementary data

Supplementary data to this article can be found online at <https://doi.org/10.1016/j.redox.2023.102843>.

References

- [1] B.I. Yamout, R. Alroughani, Multiple sclerosis, *Semin. Neurol.* 38 (2) (2018) 212–225.
- [2] S. Rodriguez Murua, M.F. Farez, F.J. Quintana, The immune response in multiple sclerosis, *Annu. Rev. Pathol.* 17 (2022) 121–139.
- [3] M. Charabati, M.A. Wheeler, H.L. Weiner, F.J. Quintana, Multiple sclerosis: neuroimmune crosstalk and therapeutic targeting, *Cell* 186 (7) (2023) 1309–1327.
- [4] L. Makowski, M. Chaib, J.C. Rathmell, Immunometabolism: from basic mechanisms to translation, *Immunol. Rev.* 295 (1) (2020) 5–14.
- [5] G. Soto-Herederro, M.M. Gomez de Las Heras, E. Gabande-Rodriguez, J. Oller, M. Mittelbrunn, Glycolysis - a key player in the inflammatory response, *FEBS J.* 287 (16) (2020) 3350–3369.
- [6] A.C. Codo, G.G. Davanzo, L.B. Monteiro, G.F. de Souza, S.P. Muraro, J.V. Virgilio-da-Silva, J.S. Prodonoff, V.C. Carregari, C.A.O. de Biagi Junior, F. Crunfli, J. L. Jimenez Restrepo, P.H. Vendramini, G. Reis-de-Oliveira, K. Bispo Dos Santos, D. A. Toledo-Teixeira, P.L. Parise, M.C. Martini, R.E. Marques, H.R. Carmo, A. Borin,

- L.D. Coimbra, V.O. Boldrini, N.S. Brunetti, A.S. Vieira, E. Mansour, R.G. Ulaf, A. F. Bernardes, T.A. Nunes, L.C. Ribeiro, A.C. Palma, M.V. Agrela, M.L. Moretti, A. C. Sposito, F.B. Pereira, L.A. Velloso, M.A.R. Vinolo, A. Damasio, J.L. Proença-Modena, R.F. Carvalho, M.A. Mori, D. Martins-de-Souza, H.I. Nakaya, A.S. Farias, P.M. Moraes-Vieira, Elevated glucose levels favor SARS-CoV-2 infection and monocyte response through a HIF-1 α /Glycolysis-Dependent Axis, *Cell Metabol.* 32 (3) (2020) 437–446.
- [7] O.R. Colegio, N.Q. Chu, A.L. Szabo, T. Chu, A.M. Rhebergen, V. Jairam, N. Cyrus, C.E. Brokowski, S.C. Eisenbarth, G.M. Phillips, G.W. Cline, A.J. Phillips, R. Medzhitov, Functional polarization of tumour-associated macrophages by tumour-derived lactic acid, *Nature* 513 (7519) (2014) 559–563.
- [8] G.M. Tannahill, A.M. Curtis, J. Adamik, E.M. Palsson-McDermott, A.F. McGettrick, G. Goel, C. Frezza, N.J. Bernard, B. Kelly, N.H. Foley, L. Zheng, A. Gardet, Z. Tong, S.S. Jany, S.C. Corr, M. Haneklaus, B.E. Caffrey, K. Pierce, S. Walsmsley, F. C. Beasley, E. Cummins, V. Nizet, M. Whyte, C.T. Taylor, H. Lin, S.L. Masters, E. Gottlieb, V.P. Kelly, C. Clish, P.E. Auron, R.J. Xavier, L.A. O'Neill, Succinate is an inflammatory signal that induces IL-1 beta through HIF-1 α , *Nature* 496 (7444) (2013) 238–242.
- [9] R. Kold-Christensen, M. Johannsen, Methylglyoxal metabolism and aging-related disease: moving from correlation toward causation, *Trends Endocrinol. Metabol.* 31 (2) (2020) 81–92.
- [10] I. Allaman, M. Belanger, P.J. Magistretti, Methylglyoxal, the dark side of glycolysis, *Front. Neurosci.* 9 (2015) 23.
- [11] T. Aki, T. Funakoshi, K. Noritake, K. Unuma, K. Uemura, Extracellular glucose is crucially involved in the fate decision of LPS-stimulated RAW264.7 murine macrophage cells, *Sci. Rep.* 10 (1) (2020), 10581.
- [12] D.E. Maessen, C.D. Stehouwer, C.G. Schalkwijk, The role of methylglyoxal and the glyoxalase system in diabetes and other age-related diseases, *Clin. Sci. (Lond.)* 128 (12) (2015) 839–861.
- [13] J. Chaudhuri, Y. Bains, S. Guha, A. Kahn, D. Hall, N. Bose, A. Gugliucci, P. Kapahi, The role of advanced glycation end products in aging and metabolic diseases: bridging association and causality, *Cell Metabol.* 28 (3) (2018) 337–352.
- [14] C. Nigro, A. Leone, F. Fiory, I. Prevenzano, A. Nicolo, P. Mirra, F. Beguinot, C. Miele, Dicarbonyl stress at the crossroads of healthy and unhealthy aging, *Cells* 8 (7) (2019) 749.
- [15] S. Wetzels, K. Wouters, T. Miyata, J. Scheijen, J.J.A. Hendriks, C.G. Schalkwijk, T. Vanmierlo, Advanced glycation endproducts are increased in the animal model of multiple sclerosis but cannot be reduced by pyridoxamine treatment or glyoxalase 1 overexpression, *Int. J. Mol. Sci.* 19 (5) (2018) 1311.
- [16] I. Knani, H. Bouzidi, S. Zrour, N. Bergaoui, M. Hammami, M. Kerkeni, Methylglyoxal: a relevant marker of disease activity in patients with rheumatoid arthritis, *Dis. Markers* 2018 (2018), 8735926.
- [17] C. Laaker, M. Hsu, Z. Fabry, S.D. Miller, W.J. Karpus, Experimental autoimmune encephalomyelitis in the mouse, *Curr Protoc* 1 (12) (2021), e300.
- [18] I.M. Stromnes, J.M. Goverman, Active induction of experimental allergic encephalomyelitis, *Nat. Protoc.* 1 (4) (2006) 1810–1819.
- [19] R.T. Liu, M. Zhang, C.L. Yang, P. Zhang, N. Zhang, T. Du, M.R. Ge, L.T. Yue, X.L. Li, H. Li, R.S. Duan, Enhanced glycolysis contributes to the pathogenesis of experimental autoimmune neuritis, *J. Neuroinflammation* 15 (1) (2018) 51.
- [20] D. Wencel, T. Abel, C. McDonagh, Optical chemical pH sensors, *Anal. Chem.* 86 (1) (2014) 15–29.
- [21] W. Yao, R.H. Byrne, Spectrophotometric determination of freshwater pH using bromocresol purple and phenol red, *Environ. Sci. Technol.* 35 (6) (2001) 1197–1201.
- [22] H. Wang, Y. Xu, L. Rao, C. Yang, H. Yuan, T. Gao, X. Chen, H. Sun, M. Xian, C. Liu, C. Liu, Ratiometric fluorescent probe for monitoring endogenous methylglyoxal in living cells and diabetic blood samples, *Anal. Chem.* 91 (9) (2019) 5646–5653.
- [23] Z. Yan, W. Qi, J. Zhan, Z. Lin, J. Lin, X. Xue, X. Pan, Y. Zhou, Activating Nrf2 signalling alleviates osteoarthritis development by inhibiting inflammasome activation, *J. Cell Mol. Med.* 24 (22) (2020) 13046–13057.
- [24] D. Prantner, S. Nallar, K. Richard, D. Spiegel, K.D. Collins, S.N. Vogel, Classically activated mouse macrophages produce methylglyoxal that induces a TLR4- and RAGE-independent proinflammatory response, *J. Leukoc. Biol.* 109 (3) (2021) 605–619.
- [25] L. Wang, S. Pavlou, X. Du, M. Bhukory, H. Xu, M. Chen, Glucose transporter 1 critically controls microglial activation through facilitating glycolysis, *Mol. Neurodegener.* 14 (1) (2019) 2.
- [26] W. Li, G. Qu, S.C. Choi, C. Cornaby, A. Titov, N. Kanda, X. Teng, H. Wang, L. Morel, Targeting T cell activation and lupus autoimmune phenotypes by inhibiting glucose transporters, *Front. Immunol.* 10 (2019) 833.
- [27] A.N. Macintyre, V.A. Gerriets, A.G. Nichols, R.D. Michalek, M.C. Rudolph, D. Deoliveira, S.M. Anderson, E.D. Abel, B.J. Chen, L.P. Hale, J.C. Rathmell, The glucose transporter Glut1 is selectively essential for CD4 T cell activation and effector function, *Cell Metabol.* 20 (1) (2014) 61–72.
- [28] M. Yamamoto, S. Yamazaki, S. Uematsu, S. Sato, H. Hemmi, K. Hoshino, T. Kaisho, H. Kuwata, O. Takeuchi, K. Takeshige, T. Saitoh, S. Yamaoka, N. Yamamoto, S. Yamamoto, T. Muta, K. Takeda, S. Akira, Regulation of Toll/IL-1-receptor-mediated gene expression by the inducible nuclear protein IkappaBzeta, *Nature* 430 (6996) (2004) 218–222.
- [29] S. Horber, D.G. Hildebrand, W.S. Lieb, S. Lorscheid, S. Hailfinger, K. Schulze-Osthoff, F. Essmann, The atypical inhibitor of NF-kappaB, IkappaBzeta, controls macrophage interleukin-10 expression, *J. Biol. Chem.* 291 (24) (2016) 12851–12861.
- [30] S. Dhamiya, A. Doerrie, R. Winzen, O. Dittrich-Breiholz, A. Taghipour, N. Kuehne, M. Kracht, H. Holtmann, IL-1-induced post-transcriptional mechanisms target overlapping translational silencing and destabilizing elements in IkappaBzeta mRNA, *J. Biol. Chem.* 285 (38) (2010) 29165–29178.
- [31] M.J. Bollong, G. Lee, J.S. Coukos, H. Yun, C. Zambaldo, J.W. Chang, E.N. Chin, I. Ahmad, A.K. Chatterjee, L.L. Lairson, P.G. Schultz, R.E. Moellinger, A metabolite-derived protein modification integrates glycolysis with KEAP1-NRF2 signalling, *Nature* 562 (7728) (2018) 600–604.
- [32] N.C. Williams, L.A.J. O'Neill, A role for the krebs cycle intermediate citrate in metabolic reprogramming in innate immunity and inflammation, *Front. Immunol.* 9 (2018) 141.
- [33] K. de Leeuw, R. Graaff, R. de Vries, R.P. Dullaart, A.J. Smit, C.G. Kallenberg, M. Bijl, Accumulation of advanced glycation endproducts in patients with systemic lupus erythematosus, *Rheumatology* 46 (10) (2007) 1551–1556.
- [34] L.A.J. O'Neill, M.N. Artyomov, Iaconate: the poster child of metabolic reprogramming in macrophage function, *Nat. Rev. Immunol.* 19 (5) (2019) 273–281.
- [35] A. Hooftman, L.A.J. O'Neill, The immunomodulatory potential of the metabolite itaconate, *Trends Immunol.* 40 (8) (2019) 687–698.
- [36] V. Lampropoulou, A. Sergushichev, M. Bambouskova, S. Nair, E.E. Vincent, E. Lognicher, L. Cervantes-Barragan, X. Ma, S.C. Huang, T. Griss, C. J. Weinheimer, S. Khader, G.J. Randolph, E.J. Pearce, R.G. Jones, A. Diwan, M. S. Diamond, M.N. Artyomov, Itaconate links inhibition of succinate dehydrogenase with macrophage metabolic remodeling and regulation of inflammation, *Cell Metabol.* 24 (1) (2016) 158–166.
- [37] X. Shi, H. Zhou, J. Wei, W. Mo, Q. Li, X. Lv, The signaling pathways and therapeutic potential of itaconate to alleviate inflammation and oxidative stress in inflammatory diseases, *Redox Biol.* 58 (2022), 102553.
- [38] A. Hooftman, S. Angiari, S. Hester, S.E. Corcoran, M.C. Runtsch, C. Ling, M. C. Ruzek, P.F. Slivka, A.F. McGettrick, K. Banahan, M.M. Hughes, A.D. Irvine, R. Fischer, L.A.J. O'Neill, The immunomodulatory metabolite itaconate modifies NLRP3 and inhibits inflammasome activation, *Cell Metabol.* 32 (3) (2020) 468–478.
- [39] M.C. Runtsch, S. Angiari, A. Hooftman, R. Wadhwa, Y. Zhang, Y. Zheng, J.S. Spina, M.C. Ruzek, M.A. Argiriadi, A.F. McGettrick, R.S. Mendez, A. Zotta, C.G. Peace, A. Walsh, R. Chirillo, E. Hams, P.G. Fallon, R. Jayamaran, K. Dua, A.C. Brown, R. Y. Kim, J.C. Horvat, P.M. Hansbro, C. Wang, L.A.J. O'Neill, Itaconate and itaconate derivatives target JAK1 to suppress alternative activation of macrophages, *Cell Metabol.* 34 (3) (2022) 487–501.
- [40] L.L. Chen, C. Morcelle, Z.L. Cheng, X. Chen, Y. Xu, Y. Gao, J. Song, Z. Li, M. D. Smith, M. Shi, Y. Zhu, N. Zhou, M. Cheng, C. He, K.Y. Liu, G. Lu, L. Zhang, C. Zhang, J. Zhang, Y. Sun, T. Qi, Y. Lyu, Z.Z. Ren, X.M. Tan, J. Yin, F. Lan, Y. Liu, H. Yang, M. Qian, C. Duan, X. Chang, Y. Zhou, L. Shen, A.S. Baldwin, K.L. Guan, Y. Xiong, D. Ye, Itaconate inhibits TET DNA dioxygenases to dampen inflammatory responses, *Nat. Cell Biol.* 24 (3) (2022) 353–363.
- [41] C.G. Peace, L.A. O'Neill, The role of itaconate in host defense and inflammation, *J. Clin. Invest.* 132 (2) (2022), e148548.
- [42] A. Girma, W. Seo, R.C. She, Antibacterial activity of varying UMF-graded Manuka honeys, *PLoS One* 14 (10) (2019), e0224495.
- [43] E.L. Mills, D.G. Ryan, H.A. Prag, D. Dikovskaya, D. Menon, Z. Zaslow, M. P. Jedrychowski, A.S.H. Costa, M. Higgins, E. Hams, J. Szpyt, M.C. Runtsch, M. S. King, J.F. McGouran, R. Fischer, B.M. Kessler, A.F. McGettrick, M.M. Hughes, R. G. Carroll, L.M. Gooty, E.V. Knatko, P.J. Meakin, M.L.J. Ashford, L.K. Modis, G. Brunori, D.C. Sevin, P.G. Fallon, S.T. Caldwell, E.R.S. Kunji, E.T. Chouchani, C. Frezza, A.T. Dinkova-Kostova, R.C. Hartley, M.P. Murphy, L.A. O'Neill, Itaconate is an anti-inflammatory metabolite that activates Nrf2 via alkylation of KEAP1, *Nature* 556 (7699) (2018) 113–117.
- [44] J.J. Galligan, J.A. Wepy, M.D. Streeter, P.J. Kingsley, M.M. Mitchener, O. R. Wauchop, W.N. Beavers, K.L. Rose, T. Wang, D.A. Spiegel, L.J. Marrett, Methylglyoxal-derived posttranslational arginine modifications are abundant histone marks, *Proc. Natl. Acad. Sci. U.S.A.* 115 (37) (2018) 9228–9233.
- [45] N. Rabbani, P.J. Thornalley, Measurement of methylglyoxal by stable isotopic dilution analysis LC-MS/MS with corroborative prediction in physiological samples, *Nat. Protoc.* 9 (8) (2014) 1969–1979.
- [46] J.L. Scheijen, C.G. Schalkwijk, Quantification of glyoxal, methylglyoxal and 3-deoxyglucosone in blood and plasma by ultra performance liquid chromatography tandem mass spectrometry: evaluation of blood specimen, *Clin. Chem. Lab. Med.* 52 (1) (2014) 85–91.
- [47] N. Rabbani, P.J. Thornalley, Dicarbonyl proteome and genome damage in metabolic and vascular disease, *Biochem. Soc. Trans.* 42 (2) (2014) 425–432.
- [48] M.P. Kalapos, The tandem of free radicals and methylglyoxal, *Chem. Biol. Interact.* 171 (3) (2008) 251–271.
- [49] T. Baumann, A. Dunkel, C. Schmid, S. Schmitt, M. Hiltensperger, K. Lohr, V. Laketa, S. Donakonda, U. Ahting, B. Lorenz-Depiereux, J.E. Heil, J. Schredelseker, L. Simeoni, C. Fecher, N. Korber, T. Bauer, N. Huser, D. Hartmann, M. Laschinger, K. Eyerich, S. Eyerich, M. Anton, M. Streeter, T. Wang, B. Schraven, D. Spiegel, F. Assaad, T. Misgeld, H. Zischka, P.J. Murray, A. Heine, M. Heikenwalder, T. Korn, C. Dawid, T. Hofmann, P.A. Knolle, B. Hochst, Regulatory myeloid cells paralyze T cells through cell-cell transfer of the metabolite methylglyoxal, *Nat. Immunol.* 21 (5) (2020) 555–566.
- [50] M.T. Fischer, R. Sharma, J.L. Lim, L. Haider, J.M. Frischer, J. Drexhage, D. Mahad, M. Bradl, J. van Horsen, H. Lassmann, NADPH oxidase expression in active multiple sclerosis lesions in relation to oxidative tissue damage and mitochondrial injury, *Brain* 135 (Pt 3) (2012) 886–899.
- [51] S.R. Ruuls, J. Bauer, K. Sontrop, I. Huijtinga, B.A. T. Hart, C.D. Dijkstra, Reactive oxygen species are involved in the pathogenesis of experimental allergic encephalomyelitis in Lewis rats, *J. Neuroimmunol.* 56 (2) (1995) 207–217.

- [52] C. Griot, M. Vandeveldel, A. Richard, E. Peterhans, R. Stocker, Selective degeneration of oligodendrocytes mediated by reactive oxygen species, *Free Radic. Res. Commun.* 11 (4–5) (1990) 181–193.
- [53] Y.S. Kim, S.U. Kim, Oligodendroglial cell death induced by oxygen radicals and its protection by catalase, *J. Neurosci. Res.* 29 (1) (1991) 100–106.
- [54] D.A. Johnson, S. Amirahmadi, C. Ward, Z. Fabry, J.A. Johnson, The absence of the pro-antioxidant transcription factor Nrf2 exacerbates experimental autoimmune encephalomyelitis, *Toxicol. Sci.* 114 (2) (2010) 237–246.
- [55] S. Saha, B. Buttari, E. Panieri, E. Profumo, L. Saso, An overview of Nrf2 signaling pathway and its role in inflammation, *Molecules* 25 (22) (2020) 5474.
- [56] M.P. Soares, M.P. Seldon, I.P. Gregoire, T. Vassilevskaia, P.O. Berberat, J. Yu, T. Y. Tsui, F.H. Bach, Heme oxygenase-1 modulates the expression of adhesion molecules associated with endothelial cell activation, *J. Immunol.* 172 (6) (2004) 3553–3563.
- [57] V. Ganesh Yerra, G. Negi, S.S. Sharma, A. Kumar, Potential therapeutic effects of the simultaneous targeting of the Nrf2 and NF-kappaB pathways in diabetic neuropathy, *Redox Biol.* 1 (1) (2013) 394–397.
- [58] E.H. Kobayashi, T. Suzuki, R. Funayama, T. Nagashima, M. Hayashi, H. Sekine, N. Tanaka, T. Moriguchi, H. Motohashi, K. Nakayama, M. Yamamoto, Nrf2 suppresses macrophage inflammatory response by blocking proinflammatory cytokine transcription, *Nat. Commun.* 7 (2016), 11624.
- [59] J. Jandova, G.T. Wondrak, Genomic GLO1 deletion modulates TXNIP expression, glucose metabolism, and redox homeostasis while accelerating human A375 malignant melanoma tumor growth, *Redox Biol.* 39 (2021), 101838.
- [60] K.V. Barinova, M.V. Serebryakova, A.K. Melnikova, M.V. Medvedeva, V. I. Muronetz, E.V. Schmalhausen, Mechanism of inactivation of glyceraldehyde-3-phosphate dehydrogenase in the presence of methylglyoxal, *Arch. Biochem. Biophys.* 733 (2023), 109485.
- [61] M.R. Das, A.K. Bag, S. Saha, A. Ghosh, S.K. Dey, P. Das, C. Mandal, S. Ray, S. Chakrabarti, M. Ray, S.S. Jana, Molecular association of glucose-6-phosphate isomerase and pyruvate kinase M2 with glyceraldehyde-3-phosphate dehydrogenase in cancer cells, *BMC Cancer* 16 (2016) 152.